We are IntechOpen, the world's leading publisher of Open Access books
Built by scientists, for scientists

6,900
Open access books available

185,000
International authors and editors

200M
Downloads

154
Countries delivered to

Our authors are among the

TOP 1%
most cited scientists

12.2%
Contributors from top 500 universities

CLARIVATE ANALYTICS
BOOK CITATION INDEX
INDEXED

WEB OF SCIENCE™

Selection of our books indexed in the Book Citation Index
in Web of Science™ Core Collection (BKCI)

Interested in publishing with us?
Contact book.department@intechopen.com

Chapter

Raman Spectroscopy and Imaging of Carbon Allotropes

Gustavo Morari do Nascimento

Abstract

Raman spectroscopy is employed to study a myriad of complex materials due to the coupling of different resonances process and microscopic resources. For instance, vibrational and electronic aspects of carbon allotropes can be deeply investigated by resonance Raman spectroscopy. By selecting the appropriate laser line, it is possible to monitor different aspects of the samples, such as the behavior of metallic or semiconducting tubes and the graphene with different layers or chemical modifications. In this chapter, the potentialities of Raman technique will be exemplified in some examples obtained in our group about the characterization of carbon nanotubes and graphene. For instance, the doping process of nanotubes, carbon tube interactions with molecular magnets, and inhomogeneity of graphene samples will be discussed.

Keywords: Raman spectroscopy, Raman imaging, carbon nanotubes, graphene, modification

1. Introduction

1.1 Nanostructures

In the recent years, the synthesis and characterization of nanomaterials have been one of the most efficacious ways to produce new materials with improved or completely new properties [1]. Their physical dimensions can be used to classify the nanomaterials in subgroups. One-dimensional (1D) nanostructures are systems in which one of the spatial dimensions has less than 100 nm, such as carbon nanotubes, metallic nanowires, or zeolites having 1D cavities (**Figure 1**). Lamellar materials are classified as two-dimensional (2D) nanostructures, because there are formed by platelets piled up in one crystallographic direction, as the graphite and clays. For materials having nanocavities or structures those follow in all directions, they are named as three-dimensional nanostructures (3D; as some zeolites). When the material is symmetric in all directions, it is considered as zero-dimensional (0D) nanostructures, as found in quantum dots, fullerenes, or cyclodextrins (**Figure 1**).

Nanostructures are systems in which at least one of the spatial dimensions is smaller than 100 nm [1]. The synthesis of controlled dimensional nanostructures and the characterization of the intrinsic and potentially peculiar properties of these nanostructures are central themes in nanoscience. The study of different nanostructures has great potential to test and understand fundamental concepts about the role of particle dimensionality on their physicochemical properties. Among the various materials studied in the literature, undoubtedly,
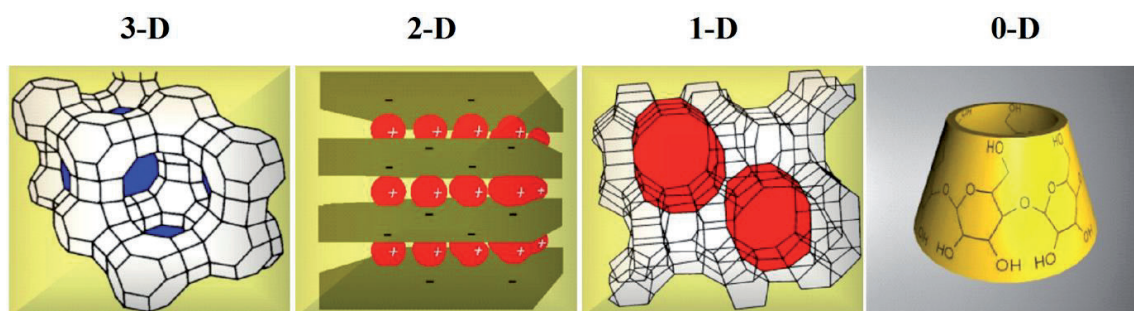
| 3-D | 2-D | 1-D | 0-D |

Figure 1.
Schematic models for 3D, 2D, 1D, and 0D materials.

carbon-derived materials, especially fullerenes and nanotubes, and more recently graphenes, are of particular note.

There are two central questions for the study of chemistry and physics of these nanostructures: (i) how controlled dimensionality nanostructures can be fabricated, and (ii) what are the intrinsic and potentially peculiar properties of these nanostructures. ID structures have great potential for testing and understanding fundamental concepts about the role of dimensionality and size over the properties. For example, 1D systems must have singularities in their electronic density of states. There are also several applications, as 1D systems are smaller structures that can be used for efficient electrical transport. Their selected properties can be explored, for example, in nanoelectronics. Among the carbon nanostructures, we highlight carbon nanotubes and graphenes [2–4].

1.2 Carbon allotropes

The discovery of fullerenes in 1985 opened a new field in chemistry [5]. Since this discovery, research with carbon structures has grown rapidly. In 1991, Sumio Iijima was the first researcher to observe some unusual carbon structures under a transmission electron microscope. Iijima called these structures as carbon nanotubes (CNTs) [2], because they consisted of many cylindrical coiled carbon layers. The layers have carbon atoms attached by six-membered rings and are stacked in the c-crystallographic direction, such as in graphite. CNTs can be open-ended or closed-ended with closed ends having five-membered carbon rings as in fullerenes.

The CNTs can be multiwalled carbon nanotubes (MWCNTs), double-walled carbon nanotubes (DWCNTs), or single-walled carbon nanotubes (SWCNTs). In fact, depending on the way, the graphite layers are coiled, i.e., the different combinations of the vectors (defined by the integers n, m) that define each tube geometrically, they can be classified as "armchair," "zigzag," and "chiral" (**Figure 2**). As consequence of this peculiar geometry, the electronic conductivity and optical properties, such as luminescence and light scattering, are dependent of the tube geometry [6–8].

CNTs attract great attention because they are model systems for nanoscience and have great potential for applications such as composite materials, batteries, sensors, and nanoscale electronics. Interest in CNTs is in their unique structure and properties, their small size (from 0.8 to 2 nm in diameter, see **Figure 1**), their ability to be metallic or semiconductor depending on their geometric structure (**Figure 2**), their exceptional ballistic transport properties and thermal conductivity, optical polarizability, and high structural perfection [6, 7].

SWCNTs have a relatively simple structure, allowing detailed calculations of their electronic structure [7, 9–12]. The unique optical properties of CNTs are due to the confinement of electronic states in one direction, resulting in the so-called
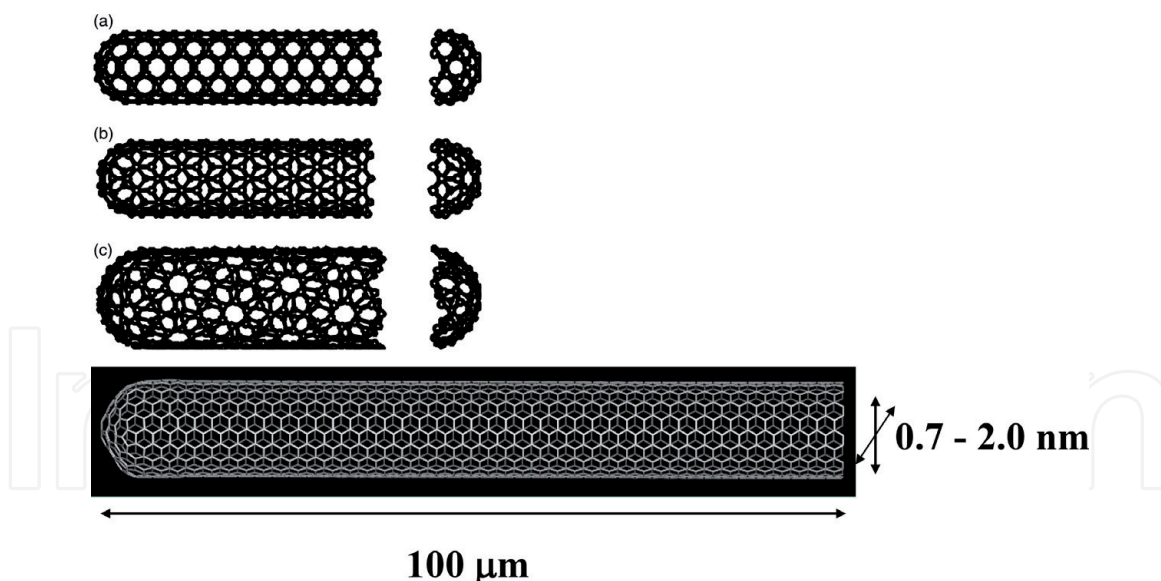
Figure 2.
Schematic models for single-axis carbon nanotubes with normal axis in (a) direction θ = 30° [tube seat (n, n)], (b) direction θ = 0° [zigzag tube (n, 0)], and (c) direction 0° < θ < 30° [chiral tube (n, m)]. The values of m and n specify a symmetry and nanotube diameter [6].

van Hove singularities [10, 13]. The presence of a large number of electron states with very close values in energy leads to an intensification of corresponding photophysical processes, and it is possible through electron absorption, photoluminescence, resonance Raman, and photoelectron spectroscopy techniques to obtain detailed information about the electronic structure and vibration analysis of nanotubes [7, 14, 15].

Theoretical predictions about the one-dimensional electronic structure of nanotubes have been experimentally verified. The most conclusive evidence comes from Scanning Tunneling Microscopy/Spectroscopy (STM/STS) studies, which showed atomic resolution images and the corresponding electronic structures for metallic and semiconductor nanotubes, and verified the dependence of electronic properties on diameter and helicity [16]. Therefore, the electronic structure of nanotubes depends only on their symmetry, being quite peculiar to solid-state physics. Specifically, the electronic structure may be metallic or semiconductor, depending on diameter and chirality, although there is no difference in the chemical bonds between carbon atoms in different nanotubes.

Despite the unique properties of CNTs, and these are already produced in macroscopic quantities, allowing the study of their physicochemical properties, they still have low solubility in most solvents, as a consequence of their high aggregation, limiting the possibility of chemical manipulation and technological application. Thus, different approaches have been employed to separate or disaggregate CNTs, such as chemical modifications of nanotubes or through interaction with polymers.

Graphite (3D), which is the most well-known allotropic form of carbon, has layers of several carbon atoms bonded with sp^2 hybridization (**Figure 3**), one carbon atom joining three other atoms forming a planar array of hexagons. The layers remain connected via the interaction of van der Waals forces. These two-dimensional sheets have the thickness of a carbon atom, which allows them to have different properties that differ from graphite, such as high electrical, thermal conductivity, and mechanical stiffness [3, 4, 18–22]. These layers have been called graphene (2D), which were discovered by scientists André Geim and Konstantin Novoselov at the end of 2004 at the University of Manchester.

Graphene is the allotropic form of carbon most recently studied, due to its wide application in the scientific environment. This material is obtained via graphite
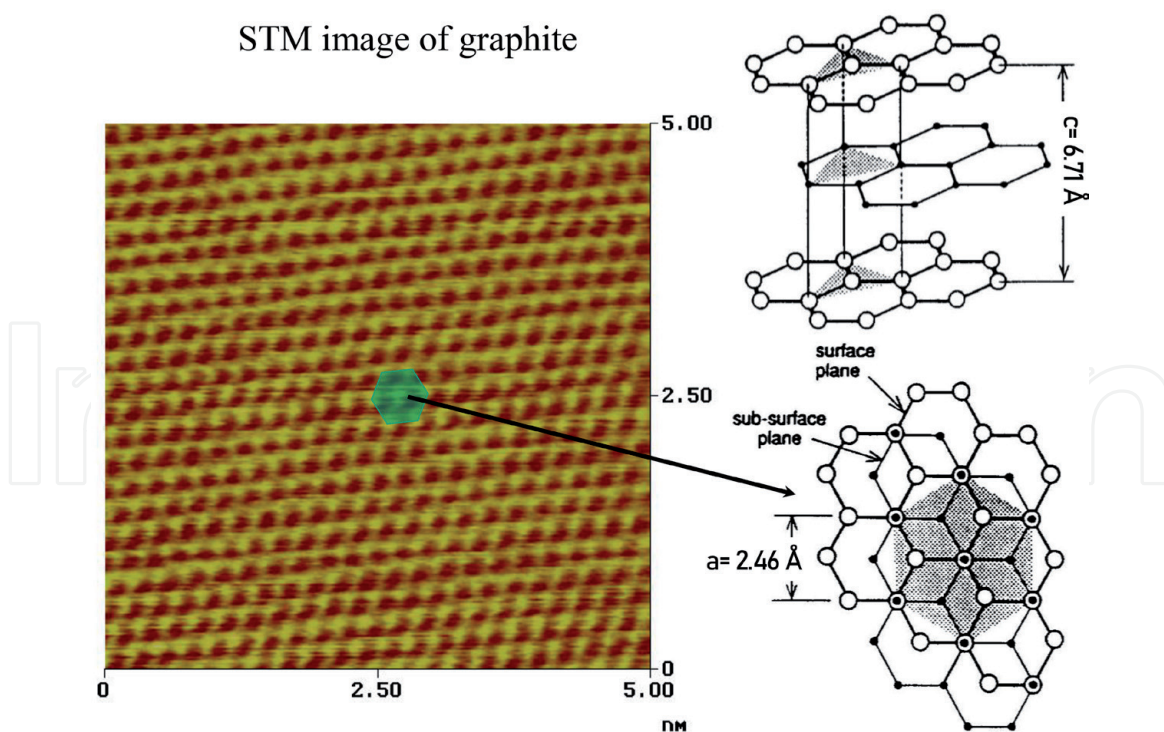
Figure 3.
STM image obtained from a HOPG crystal and the schematic models for the crystalline graphite. The crystallographic parameters were obtained from Ref. [17].

oxidation and exfoliation processes. Depending on the synthesis parameters (oxidant type, reactant proportions, temperature, etc.), graphene sheets or their oxide (GO) or graphene oxide will have distinct properties. Brodie performed the first documented synthesis in 1859 [23]. Since then, several other scientists have prepared graphene oxide (GO) synthesis experiments from graphite (G) in order to reduce the environmental hazards that this synthesis presents in the use of strong oxidants and concentrated acids. Modifications were later made by Staudenmaier (1898), who focused on improving the reaction introduced H_2SO_4 to the mixture and some aliquots of solid $KClO_3$ throughout the reaction. With these modifications, the author achieved the synthesis of a more oxidized graphic material and a simplification in the reaction [24]. However, there is release of ClO_2 gas, with risks of explosions during the process. In 1958, Hummers proposed some more modifications to this synthesis with the intention of making it safer and more profitable, replacing the oxidizing agent used in the Brodie method with MnO_4 and an additive, $NaNO_3$. All the methods mentioned so far make use of strong and toxic reagents for the production of GO, however the use of thermal expansion of graphite, or sonic spacing, those are more green routes, it takes around 6–12 h of preparation.

1.3 Raman spectroscopy and imaging

Through the years, the infrared and Raman spectroscopies have been the techniques *par excellence* for the investigation of the vibrational structure of conjugated materials, such as dyes [25], metallic complexes [26–28], conducting polymers [29, 30], nanocomposites [31–33], and carbon allotropes [34–39]. The laser is the common source in Raman spectroscopy, the radiation interacts with the sample through the scattering process. The incident light (laser source) has much more energy than the vibrational levels, however, by the scattering process; the information about the vibrational modes can be accessed. This behavior is very different

from the IR vibrational spectroscopy, where the radiation energies have the same magnitude of vibrational levels, and by absorption process, the vibrational modes can be studied (**Figure 4**).

The intensities of the Raman bands are proportional to the fourth power of the scattered frequency λ_s^4 when the laser energy is very far from a permitted molecular electronic transition [40, 41]. This behavior changes dramatically when the laser energy is close to an electronic transition, this condition is known as Resonance Raman. Hence, the intensities of the vibrational modes associated with the excited electronic state in resonance are amplified by 10^{5-7} times. For multichromophoric systems, like conducting polymers, it is possible to screen the different chromophores, just by selecting the appropriated laser line energy.

In recent years, the use of Raman spectrometers coupled with different microscopes, from optical to force atomic type, has increased. In **Figure 5**, the configuration of an optical microscope coupled to a laser source used for Raman measurements is schematically illustrated. The laser lines reach to the sample on the microscope stage by optical elements. The Raman scattered radiation is collected in a scattering angle of 180° by the same microscope objective and captured by an opening of the spectrometer using a beam splitter. It is necessary that the instrument has a high lighting efficiency, and the collection of scattered radiation must be precisely done, owing to the very small Raman cross section (typically a factor of 10^{-6} to 10^{-12} of the incident radiation) and the small volume of the sample. Raman microscopy can be considered a nondestructive technique; however, sometimes the laser power can destroy the sample or change its structure during the measurement. The use of microscopy opens the possibility to search different areas of the sample. In a conventional microscope, it is possible to investigate a very small part of the
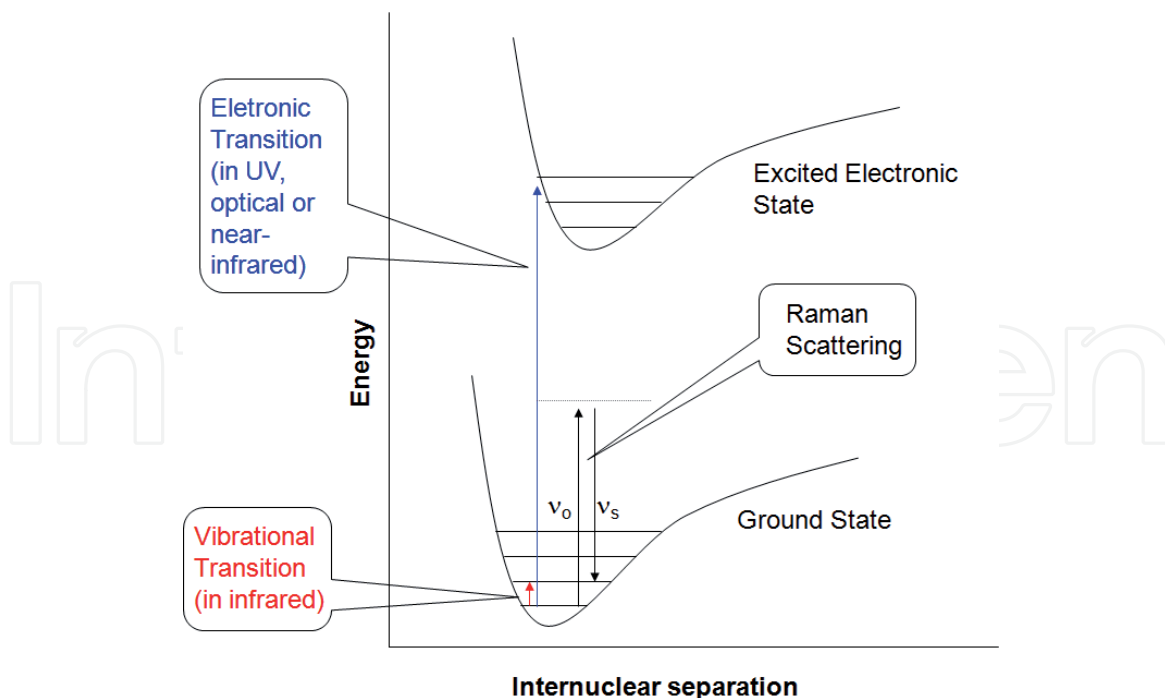
Figure 4.
Schematic representation of two electronic states (ground and excited) and their respective vibrational levels (the electronic and vibrational levels are not in the same scale). The arrows indicated the types of transitions among the different levels. For Raman scattering, if the laser line (wavenumber is represented by ν_0) has energy similar to one electronic transition of the molecule, the signal can be intensified by resonance process, known as resonance Raman effect. In the figure, ν_0 and ν_s (the scattered frequency is composed of ν_{evgm} and ν_{evgn}, the stoke and antistoke components, respectively) are the laser line and the scattered frequencies, respectively (for illustration purposes, just the stokes, $\nu_s < \nu_0$, component is shown in the diagram).
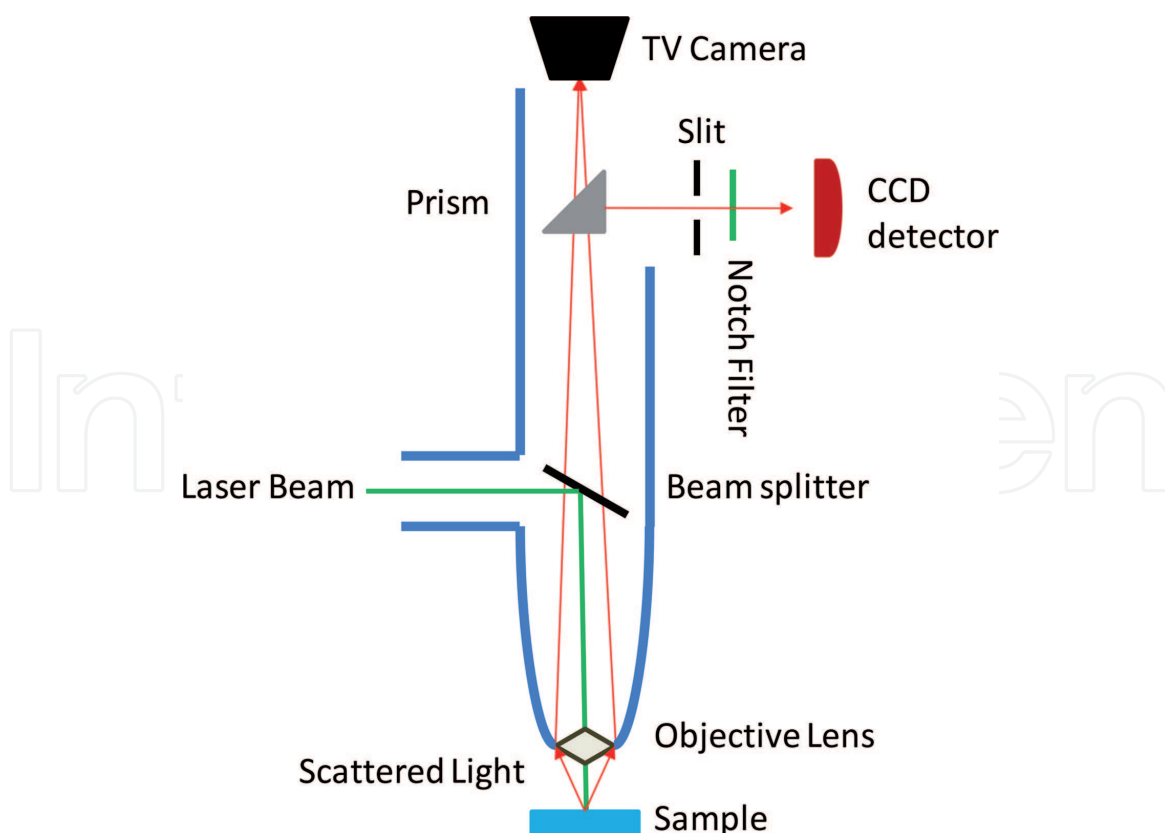
Figure 5.
Conventional Raman microscope.

sample (1 μm approximately or smaller). The high lateral resolution and depth of field (the order of a few micrometers) are very useful for the study of multilayered polymeric thin films or other complex materials [42–44].

2. Results and discussion

2.1 Resonance Raman of modified single- and double-walled carbon nanotubes

The resonance Raman spectroscopy technique is sensitive to the electronic, structural, and vibrational properties of CNTs. Our group is using resonance Raman spectroscopy to characterize the interactions between nanotubes and different kinds of molecules [25–39], such as the conducting polyaniline (PANI), molecular magnets such as $(NBu_4)_2[Cu(opba)]$, $[MnCu(opba)]_n$ chains, where opba = *ortho*-phenylenebis(oxamate), dyes such as phenosafranine (PS) and Nile Blue (NB), and CNTs doped with bromine or iodine.

For all samples investigated, the resonance Raman spectra are dominated by SWCNT or DWCNT bands at different laser excitation energies (E_{laser}) [37–39]. The Raman spectra obtained with laser lines from 790 to 514.5 nm (E_{laser} from 1.57 to 2.41 eV) are dominated by the characteristic bands from the SWCNTs or DWCNTs. This behavior is associated with the strong resonance Raman with the van Hove singularities of the single-walled nanotubes [6, 7]. The spectra can be divided into four groups of bands: (1) sharp bands from 120 to 350 cm^{-1} are assigned to the radial breathing modes (RBMs); (2) strong band in the frequency range from 1500 to 1650 cm^{-1} is attributed to stretching modes of carbon atoms (tangential G band); (3) the mode at ca. 1300–1350 cm^{-1} is forbidden for symmetry reasons and is related to the disorder-induced D-band feature; and (4) finally, the second-order

G' band (or 2D band), which is the highly dispersive harmonic of the *D*-band frequency, and it is observed here from ca. 2600 to 2700 cm^{-1}.

As a consequence of the intense CNT bands, the analysis remains in the comparison of standard CNTs before and after any chemical change. For instance, **Figure 6** exhibits the Raman spectra, in the RBM region, obtained for the composite between the SWNTs and [MnCu(opba)]$_n$ chains. At higher E_{laser} (2.33 eV) or 532.0 nm, it was observed many changes in the RBM bands, shifts from 254 to 257 cm^{-1} (Δ = +3 cm^{-1}), from 266 to 270 cm^{-1} (Δ = +4 cm^{-1}), and from 276 to 281 cm^{-1} (Δ = +5 cm^{-1}) were seen for tubes assigned to E_{11}^M family with minor diameter than observed for the other laser lines. In **Figure 6**, it is also observed that RBM bands assigned to E_{33}^S family also have changed their intensities and frequencies from 155 to 160 cm^{-1} (Δ = +5 cm^{-1}) and from 143 to 149 cm^{-1} (Δ = +6 cm^{-1}) in the presence of the heterobimetallic complex.

At E_{laser} = 2.33 eV also, semiconducting tubes interact with the heterobimetallic polymer, contrarily to that observed for lower E_{laser} energies. Hence, the RBM data suggest that the heterobimetallic polymer interacts mainly with metallic tubes independently of the diameter of the tube and excitation energy, however, for semiconducting tubes, solely for tubes with diameter higher than ca. 1.47 nm (**Figure 5**). In certain circumstances, it is possible to use UV laser line, and some bands from the metallic complex emerge in the spectra. For instance, the resonance Raman spectra, at higher E_{laser} (3.82 eV), of SWCNTs-(NBu$_4$)$_2$[Cu(opba)] samples show bands at 1430 and 1474 cm^{-1}. These bands can be assigned to the vibrational modes related to the benzene-like ring in the molecular structure of the [Cu(opba)]$^{2-}$ anion [34].

The CNT families are assigned by using the Kataura plot (**Figure 7a**). The Kataura plot is the result of calculated energy separations between the van Hove singularities [$E_{ii}(d_t)$] for SWCNTs obtained from tight-binding calculations [15, 45]. For instance, according to the Kataura plot, at 514.5 nm (E_{laser} = 2.41 eV) or 532.0 nm (E_{laser} = 2.33 eV), the DWCNTs in resonance have inner tube metallic and outer tube semiconducting. The Br$_2$ doping was reported for SWCNTs [47, 48] and for DWCNTs [49, 50]. A very large Raman bands upshifted at 514.5 nm (2.41 eV)
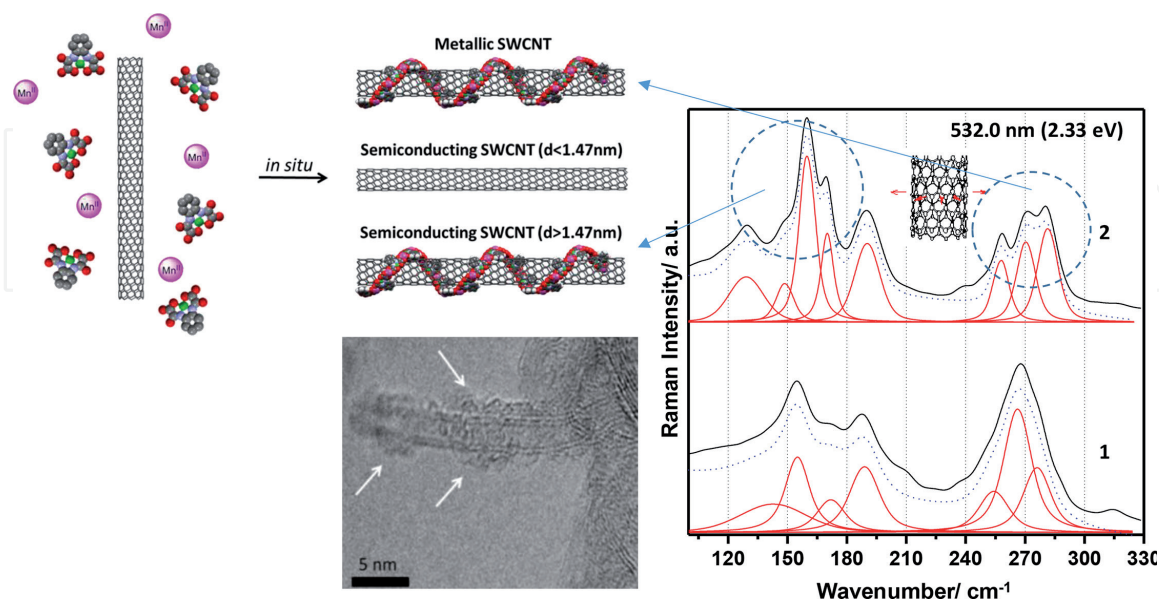
Figure 6.
Schematic representation of the selective interaction scheme between CNTs and [MnCu(opba)]$_n$ chains formed from the reaction of Cu(opba)$^{2-}$ and Mn^{2+} ions. The wrapping is selective for metallic tubes and for semiconducting with diameter higher than 1.47 nm (the HR-TEM, high resolution transmission microscopy, image of the nanocomposite is also given in the figure). Resonance Raman spectra (RBM band region) excited by laser line at 532.0 nm (2.33 eV) for powder samples 1 (DWCNTs) and 2 ([MnCu(opba)]$_n$-SWCNT materials).
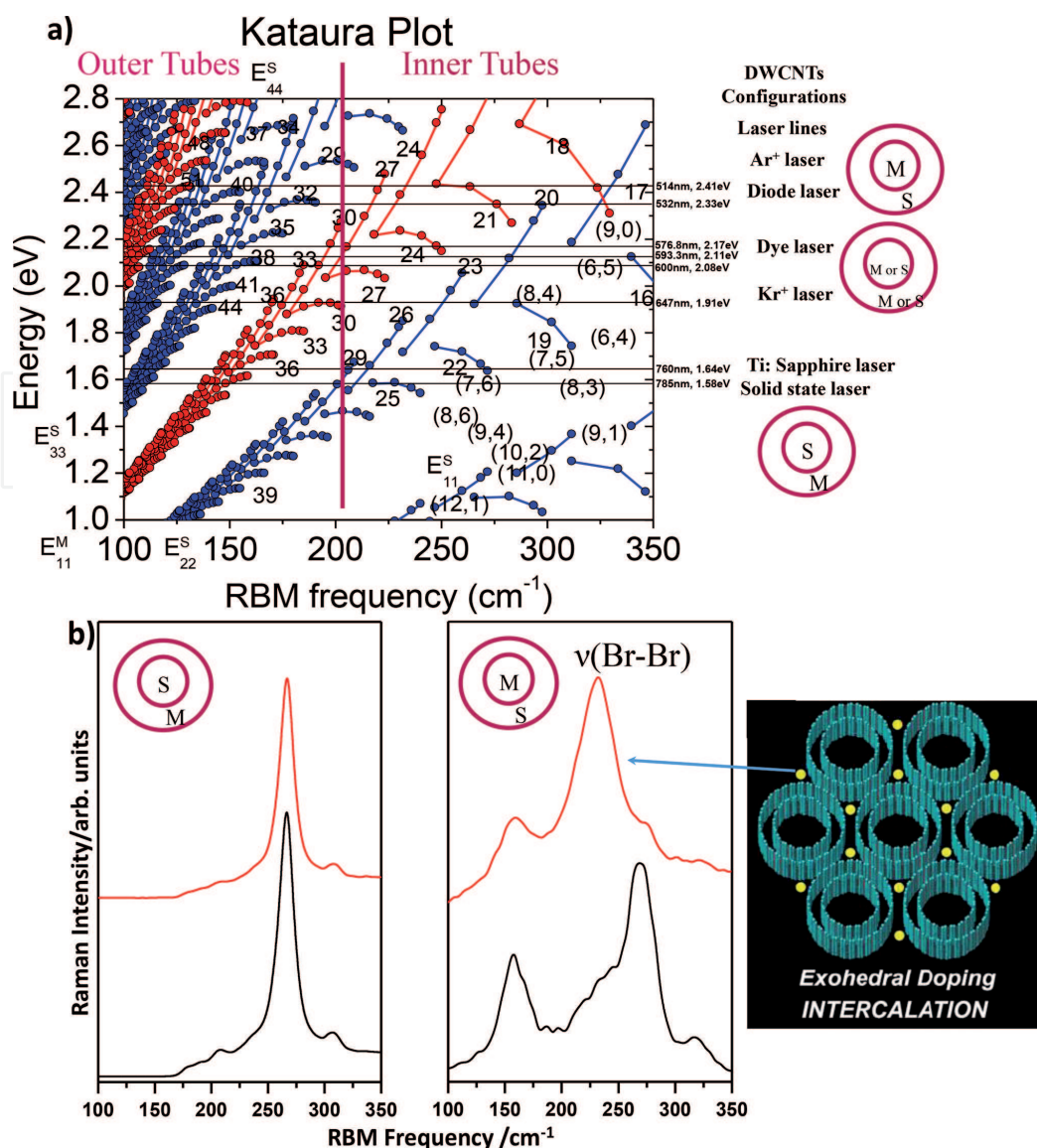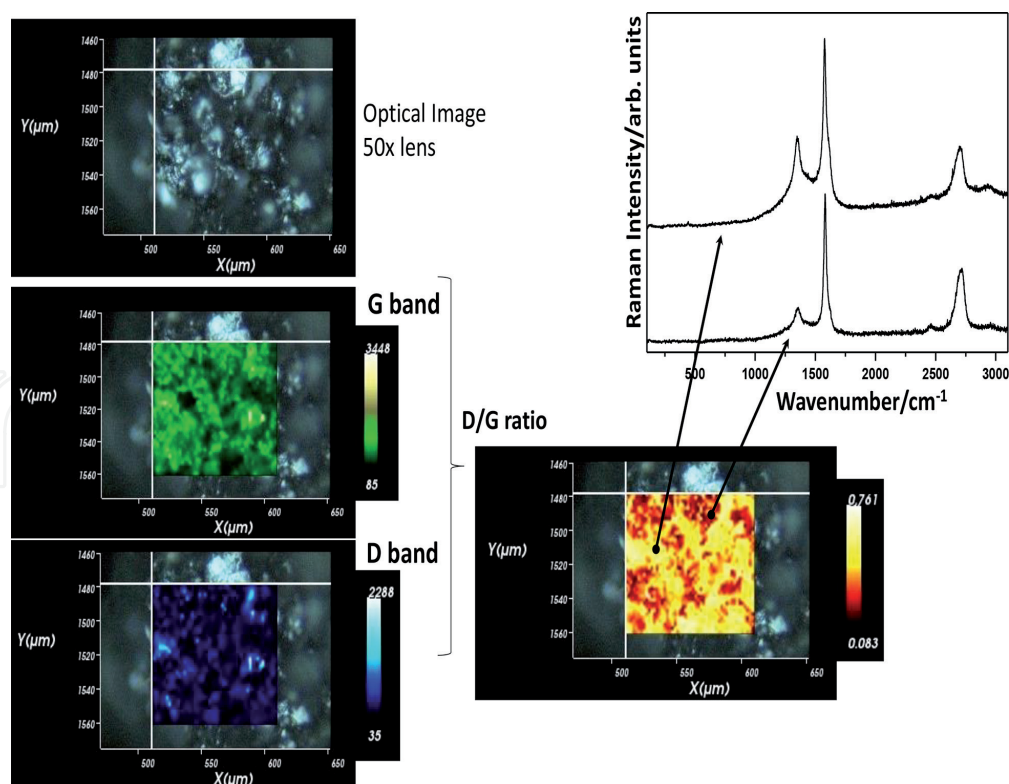
Figure 7.
(a) The Kataura plot at RBM region is based on the extended tight binding model for SWCNTs [15, 45, 46]. The horizontal lines show the laser lines used in the experiments. The numbers indicate the 2n+m families. Red circles correspond to metallic white blue to semiconducting tubes. The diameters of the tubes can be calculated by using the expression $\nu_{RBM} = 233/dt + 14$ [46]. (b) Resonance Raman spectra at 532.0 nm (2.33 eV) of DWCNTs before and after doping (black and red lines, respectively) with 31 wt% of Br_2. For illustrative purpose, the schematic representation of the exohedral doping is also given in the figure.

laser line in both the RBM and G^+ band for brominated SWCNTs are observed. Indeed, the doping induces a Fermi level depression of 1.2–1.4 eV in the DWCNTs after bromination, mainly in the outer tubes. The Br–Br molecular vibration is reduced to ca. 233 cm^{-1} in comparison with molecular bromine (323 cm^{-1}) [37–39], as a consequence to the charge transfer with the carbon tubes.

The use of a large variety of laser lines [37–39] permits to monitor differences in the charge transfer behavior to the inner and outer tubes from the adsorbed bromine or iodine. **Figure 7b** shows that the Br_2 molecules are interacting with the outer tube surface of the DWCNTs and that the adsorbed bromine molecules act as an electron acceptor. In addition, it is observed that metallic tubes are extremely sensitive to doping process. In fact, the presence of Br_2 molecules changes the Raman spectra of the metallic tubes even when they are in the inner configuration surrounded by semiconducting outer tubes of DWCNTs.

The differences between metallic and semiconducting tubes can also be analyzed in the other regions of the Raman spectra of CNTs. For instance, the presence of the lower frequency component of the *G*-band spectra is associated with the

Figure 8.
Resonance Raman imaging of commercial samples of graphene. The images on left are from the top: optical image obtained with a 50× lens, the Raman imaging using the G band as intensity marker (green image), and the Raman imaging using the D band as intensity marker (blue image). In addition, the Raman imaging obtained from D/G ratio is also given (red-yellow image) and the corresponding resonance Raman spectra from red and yellow regions.

metallic tubes. This is the result of the strong electron-phonon coupling observed in metallic nanotubes, and it gives rise to Kohn anomalies in the phonon dispersions [51, 52]. Hence, the influence of the metallic tubes can easily be distinguished from semiconducting G^- feature, which shows a Breit-Wigner-Fano (BWF) line shape [53, 54]. The changes in relative intensities, dispersion, and linewidth of the G' (2D) band can also be used as a probe to extract information about interactions between the tubes and the graphene layers.

2.2 Raman imaging of commercial sample of graphene

More recently, our group is dedicated to prepare modified graphene samples with a myriad of molecules. However, due to the limitations of chemical procedures for the preparation of chemically modified graphene, the resulting samples are very inhomogeneous. Graphene consists in a two-dimensional single-layer sheet of sp^2 hybridized carbon atoms having excellent electron transport properties and very high carrier mobility and thermal conductivity. However, the interesting properties exhibited by graphene are only observed for graphene films that contain only one or a few graphene layers [3, 4]. It is optically difficult to observe low number of layers, but single-, double-, and multilayer graphenes can be differentiated by their Raman fingerprints. The graphene Raman spectrum is dominated by G band (ca. 1582 cm^{-1}) and 2D band (ca. 2685 cm^{-1}). Ferrari and coworkers [55] used Raman to characterize samples consisting of varying number of graphene layers and found that the 2D band width and shape modify with increasing the number of layers. Therefore, the spectral shape of the 2D band is representative of the number of graphene layers and can be used to determine that number. By using

Raman imaging has been possible to analyze a large area of the graphene samples in order to search irregularities. For example, **Figure 8** shows the Raman imaging obtained from a commercial sample of graphene (Sigma-Aldrich). The D- and G-band intensities were used as probe to see the differences in a large area of the sample.

The D and G images can be combined to form an image from the D/G ratio of intensities (red-yellow image). The Raman spectra of two spots of the sample exemplify the point; yellow regions have more intense D bands than red regions.

3. Conclusion and future remarks

The screening of the electronic and vibrational structure of carbon allotropes through Raman spectroscopy has been decisive in determination of their structure and in the study of the interactions between the carbon allotropes with a myriad of other molecules. In fact, by selecting the appropriate laser line, it is possible to study in particular metallic or semiconducting tubes or monolayer graphenes. The new Raman instruments can give better Raman imaging of the samples and open the possibility to study inhomogeneity, chemical modifications, and many other aspects of the carbon samples in a large area.

Author details

Gustavo Morari do Nascimento
Federal University of ABC, Santo André, Brazil

*Address all correspondence to: Gustavo.morari@ufabc.edu.br; morari@yahoo.com

IntechOpen

References

[1] Ozin GA, Arsenault AC. Nanochemistry: A Chemical Approach to Nanomaterials. Cambridge: RSC Publishing; 2005

[2] Ijima S. Helical microtubules of graphitic carbon. Nature. 1991;**354**:56

[3] Novoselov KS, Geim AK, Morozov SV, Jiang D, Zhang Y, Dubonos SV, et al. Electric field effect in atomically thin carbon films. Science. 2004;**306**:666

[4] Geim AK, Novoselov KS. The rise of graphene. Nature Materials. 2007;**6**:183

[5] Kroto HW, Heath JR, O'Brien SC, Curl RF, Smalley RE. C60: Buckminsterfullerene. Nature. 1985;**318**:162

[6] Saito R, Dresselhaus G, Dresselhaus MS. Physical Properties of Carbon Nanotubes. London: Imperial College Press; 1998

[7] Dresselhaus MS, Dai H. Carbon nanotubes: Continued innovations and challenges. MRS Bulletin. 2004;**29**:237

[8] Jorio A, Saito R, Hertel T, Weisman RB, Dresselhaus G, Dresselhaus MS. Carbon nanotube photophysics. MRS Bulletin. 2004;**29**:276

[9] Saito R, Fujita M, Dresselhaus G, Dresselhaus MS. Electronic structure of graphene tubules based on C60. Physical Review B. 1992;**46**:1804

[10] Mintmire JW, Robertson DH, White CT. Properties of fullerene nanotubules. Journal of Physics and Chemistry of Solids. 1993;**54**:1935

[11] Ijima S, Ichihashi T. Single-shell carbon nanotubes of 1-nm diameter. Nature. 1993;**363**:603

[12] Bethune DS, Kiang CH, de Vries MS, Gorman G, Savoy R, Vazquez J, et al. Cobalt-catalysed growth of carbon nanotubes with single-atomic-layer walls. Nature. 1993;**363**:605

[13] Dresselhaus MS, Dresselhaus G, Avouris P. Carbon Nanotubes: Synthesis, Structure, Properties and Applications. Berlin: Springer-Verlag; 2001

[14] Dresselhaus MS, Dresselhaus G, Jorio A, Souza Filho AG, Pimenta MA, Saito R. Single nanotube Raman spectroscopy. Accounts of Chemical Research. 2002;**35**:1070

[15] Jorio A, Saito R, Hafner JH, Lieber CM, Hunter M, McClure T, et al. Structural (n,m) determination of isolated single-wall carbon nanotubes by resonant Raman scattering. Physical Review Letters. 2001;**86**:1118

[16] Qujang M, Huang J-L, Lieber CM. Fundamental electronic properties and applications of single-walled carbon nanotubes. Accounts of Chemical Research. 2002;**35**:1018

[17] Chung D. Review: graphite. Journal of Materials Science. 2002;**37**:1475

[18] Rao CNR, Sood AK, Subrahmanyam KS, Govindaraj A. Graphene: the new two-dimensional nanomaterial. Angewandte Chemie, International Edition. 2009;**48**:7752

[19] Pati SK, Enoki T, Rao CNR. Graphene and its Fascinating Attributes. Singapore: World Scientific; 2011

[20] Wallace PR. The band theory of graphite. Physics Review. 1947;**71**:622

[21] Dreyer DR, Ruoff RS, Bielawski CW. From conception to realization: An historical account of graphene and some perspectives for its future. Angewandte

Chemie, International Edition. 2010;**49**:9336

[22] Novoselov KS, Jiang D, Schedin F, Booth TJ, Khotkevich VV, Morozov SV, et al. Proceedings of the National Academy of Sciences of the United States of America. 2005;**102**:10451

[23] Pendolino F, Armata N. Graphene Oxide in Environmental Remediation Process. 1st ed. Itália: Springer; 2017

[24] Hummers S, Offeman RE. Preparation of graphitic oxide. Journal of the American Chemical Society. 1958;**80**(6):1339

[25] Bonancea CE, do Nascimento GM, de Souza ML, Temperini MLA, Corio P. Substrate development for surface-enhanced Raman study of photocatalytic degradation processes: Congo red over silver modified titanium dioxide films. Applied Catalysis B: Environmental. 2006;**69**:34-42

[26] Silva IF, Teixeira IF, Barros WP, Pinheiro CB, Ardisson JD, do Nascimento GM, et al. An FeIII dinuclear metallacycle complex as a sizeselective adsorbent for nitrogenous compounds and a potentially effective ammonia storage material. Journal of Materials Chemistry A. 2019;**7**:15225-15232

[27] do Nascimento GM, do Pim WD, Reis DO, Simoes TRG, Pradie NA, Stumpf HO. Characterization of compounds derived from copper-oxamate and imidazolium by X-ray absorption and vibrational spectroscopies. Spectrochimica Acta Part A. 2015;**142**:303-310

[28] do Nascimento GM, Corio P, Novickis RW, Temperini MLA, Dresselhaus MS. Synthesis and characterization of single-wall-carbon-nanotube-doped emeraldine salt and base polyaniline nanocomposites. Journal of Polymer Science, Part A: Polymer Chemistry. 2005;**43**:815

[29] do Nascimento GM, Silva TB, Corio P, Dresselhaus MS. Charge-transfer behavior of polyaniline single wall carbon nanotubes nanocomposites monitored by resonance Raman spectroscopy. Journal of Raman Specroscopy. 2010;**41**:1587

[30] do Nascimento GM, Constantino VRL, Temperini MLA. Spectroscopic characterization of a new type of conducting polymer-clay nanocomposite. Macromolecules. 2002;**35**:7535

[31] do Nascimento GM, Constantino VRL, Temperini MLA. Spectroscopic characterization of doped poly(benzidine) and its nanocomposite with cationic clay. The Journal of Physical Chemistry B. 2004;**108**:5564

[32] do Nascimento GM, Constantino VRL, Landers R, Temperini MLA. Aniline polymerization into montmorillonite clay: A spectroscopic investigation of the intercalated conducting polymer. Macromolecules. 2004;**37**:9373

[33] Do Nascimento GM, do Pim WD, Endo M, Choi GB, Kim YA, Pradie NA, et al. Single-wall carbon nanotube modified with copper-oxamate flat complex probed by synchrotron x-ray photoelectron and x-ray absorption spectroscopies. Journal of Molecular Structure. 2019;**1176**:711-719

[34] Silva IF, do Pim WD, Teixeira IF, Barros WP, Teixeira APC, Do Nascimento GM, et al. Selective wrapping of few-walled carbon nanotubes by a serpent-like heterobimetallic coordination polymer. Journal of Physical Chemistry C. 2016;**120**:1245

[35] do Nascimento GM, Barros WP, Kim YA, Muramatsu H, Hayashi T, Endo M, et al. Single-wall carbon nanotube interactions with copper-oxamato building block of

moleculebased magnets probed by resonance Raman spectroscopy. Journal of Raman Specroscopy. 2012;**43**:1951

[36] do Nascimento GM, de Oliveira RC, Pradie NA, Lins PRG, Worfel PR, Martinez GR, et al. Single-wall carbon nanotubes modified with organic dyes: Synthesis, characterization and potential cytotoxic effects. Journal of Photochemistry and Photobiology A: Chemistry. 2010;**211**(2-3):99-107

[37] do Nascimento GM, Hou T, Kim YA, Muramatsu H, Hayashi T, Endo M, et al. Behavior of the high frequency Raman modes of double-wall carbon nanotubes after doping with bromine or iodine vapors. Carbon. 2011;**49**:3585-3596

[38] do Nascimento GM, Hou T, Kim YA, Muramatsu H, Hayashi T, Endo M, et al. Double-wall carbon nanotubes doped with different Br2 doping levels: A resonance Raman study. Nano Letters. 2008;**8**(12):4168-4172

[39] do Nascimento GM, Hou T, Kim YA, Muramatsu H, Hayashi T, Endo M, et al. Comparison of the resonance raman behavior of double-walled carbon nanotubes doped with bromine or iodine vapors. Journal of Physical Chemistry C. 2009;**113**(10):3934-3938

[40] Nakamoto N, Ferraro JR. Introduction to Raman Spectroscopy. London: Academic Press, Inc.; 1994

[41] Rostron P. D. Gerber Raman spectroscopy, a review. International Journal of Engineering and Technical Research. 2016;**6**:50-64

[42] Batchelder DN. In: Brässler H, editor. Optical Techniques to Characterize Polymer Systems. Amsterdam: Elsevier; 1987

[43] Batchelder DN, Bloor D. In Advances in Infrared and Raman Spectroscopy. Wiley-Heyden: London; 1984

[44] Clark JH, Dines TJ. Resonance raman spectroscopy, and its application to inorganic chemistry. New Analytical Methods (27). Angewandte Chemie (International Ed. in English). 1986;**25**:131

[45] Kataura H, Kumazawa Y, Maniwa Y, Umezu I, Suzuki S, Ohtsuka Y, et al. Optical properties of single-wall carbon nanotubes. Synthetic Metals. 1999;**103**(1-3):2555-2558

[46] Pfeiffer R, Kramberger C, Simon F, Kusmany H, Popov VN, Kataura H. Interaction between concentric tubes in DWCNTs. European Physical Journal B. 2004;**42**:345-350

[47] Lee RS, Kim HJ, Fischer JE, Thess A, Smalley RE. Conductivity enhancement in single-walled carbon nanotube bundles doped with K and Br. Nature. 1997;**388**(6639):255-257

[48] Rao AM, Eklund PC, Bandow S, Thess A, Smalley RE. Evidence for charge transfer in doped carbon nanotube bundles from Raman scattering. Nature. 1997;**388**(6639):257-259

[49] Chen G, Bandow S, Margine ER, Nisoli C, Olmogorov AN, Crespi VH, et al. Chemically doped double-walled carbon nanotubes: Cylindrical molecular capacitors. Physical Review Letters. 2003;**90**(25):257403-257404

[50] Souza Filho AG, Endo M, Muramatsu H, Hayashi T, Kim YA, Barros EB. et al. Resonance Raman scattering studies in Br2-adsorbed double-wall carbon nanotubes. Physical Review B.2006;**73**(23):235413-235411-12

[51] Piscanec S, Lazzeri M, Robertson J, Ferrari AC, Mauri F. Optical phonons in carbon nanotubes: Kohn anomalies, Peierls distortions, and dynamic effects. Physical Review B. 2007;**75**(3):035427

[52] Basko DM, Piscanec S, Ferrari AC. Electron–electron interactions and doping dependence of the two-phonon Raman intensity in graphene. Physical Review B.2009;**80**(16):165413- 165411-10

[53] Souza Filho AG, Jorio A, Samsonidze GG, Dresselhaus G, Pimenta MA, Dresselhaus MS et al. Competing spring constant versus double resonance effects on the properties of dispersive modes in isolated single-wall carbon nanotubes. Physical Review B.2003;**67**(3):035427- 035421-7

[54] Jorio A, Souza Filho AG, Dresselhaus G, Dresselhaus MS, et al. G-band resonant Raman study of 62 isolated single-wall carbon nanotubes. Physical Review B. 2002;**65**(15):155412-155419

[55] Ferrari AC, Meyer JC, Scardaci V, Casiraghi C, Lazzeri M, Mauri F, et al. Raman spectrum of graphene and graphene layers. Physical Review Letters. 2006;**97**:187401